

# A CONCURRENT TWO-SCALE APPROACH FOR HIGH STRENGTH CONCRETE

LUIS A. G. BITENCOURT JR.<sup>†</sup>, MARCELA GIMENES<sup>\*</sup>, EDUARDO A. RODRIGUES<sup>\*</sup>  
AND OSVALDO L. MANZOLI<sup>\*</sup>

<sup>†</sup>University of São Paulo (USP)  
Department of Structural and Geotechnical Engineering  
Av. Prof. Almeida Prado, trav. do Biênio, 83, 05508-070, Cidade Universitária, São Paulo, Brazil  
e-mail: [luis.bitencourt@usp.br](mailto:luis.bitencourt@usp.br)

<sup>\*</sup> São Paulo State University (UNESP)  
Department of Civil Engineering  
Av. Eng. Luís Edmundo Carrijo Coube, 14-01, Bauru, Brazil  
e-mail: [osvaldo.l.manzoli@unesp.br](mailto:osvaldo.l.manzoli@unesp.br); [marcela.gimenes@unesp.br](mailto:marcela.gimenes@unesp.br); [eduardo.alexandre@unesp.br](mailto:eduardo.alexandre@unesp.br)

**Keywords:** High Strength Concrete; Mesoscale Model; Fragmentation Technique; Coupling Finite Element.

**Abstract:** The present work proposes a concurrent two-scale (macro and mesoscale) approach for HSC, in which a linear elastic model with homogenized elastic properties is used for the macroscale and a three-phase material composed of coarse aggregate, mortar matrix and the interfacial transition zone (ITZ) with nonlinear behavior models are assumed for the mesoscopic level. The coarse aggregates are randomly generated from a certain grading curve and placed in the mesoscale subdomain, using the “take-and-place” method. The mesh fragmentation technique is employed, as proposed by Manzoli et al. [13]. This technique is based on the use of interface finite elements with high aspect ratio, which along with the employment of a constitutive tensile damage model is able to represent the crack initiation, propagation and coalescence, considering the individual behavior of each phase as well as their mutual interactions in the mesoscale HSC. The macroscopic and mesoscopic meshes are attached via coupling finite elements, which provide a rigid coupling between them. Dog-bone specimens and three-point bending tests with different aggregate size distributions are numerically simulated. The results showed that the proposed approach is a promising methodology and may be useful for modeling crack propagation in concretes with different strengths.

## 1 INTRODUCTION

The use of concretes which exceed 50 MPa becomes more common as it results in an increased performance mainly in terms of strength and durability. For a long time, researches on high strength concrete (HSC) were mainly focused on developing technologies that would grant an increased strength to it [1-2]. The main difference in the composition of HSC and the normal strength concrete (NSC) are the pozzolanic materials (such as fly ash and silica fume) added to the mix, granting additional

strength by reacting with cement hydration products to create additional Calcium-Silicate-Hydrate gel, the part of the paste responsible for concrete strength [3].

In addition, to its superior and earlier compressive strength, the HSC also exhibits a particular fracture behaviour, as it has a less porous and more compact mortar matrix whose compressive and tensile strength might equate to the values of rock aggregates [4]. For that reason, nowadays it is observed that much research is focused on understanding the mechanical particularities of that composite material. For

example, experimental tests were performed evaluating the HSC fracture behavior under varied loading rates, made from varied rock compositions, with different aggregate size or volume of aggregates. Most of the authors agree that the impact of the coarse aggregate type on the strength of concrete is more significant in HSC [4-6].

At the mesoscopic level, the fracture behavior of HSC can differ significantly from the conventional strength concrete since the coarse aggregate may be the weakest phase of the composite. The fracture propagation, as opposed to what happens in the conventional concrete, might cut aggregate sections. Therefore, coarse aggregate type, size, and distribution can also affect all the macroscopic mechanical responses, such as the ultimate tensile strength and fracture energy [5-6].

For what concerns the HSC simulation, with the advance in computer resources, numeric models are now able to consider the internal structure of this heterogeneous material by differentiating aggregates, mortar, ITZs and even pores and weak inclusions [7-9]. By using such tools, one can expect more accurate insights on the material mechanical behaviour. Mesoscale models, in particular, have been successfully employed to represent the material structure in reduced scale experiments [7-11]. The results obtained from these studies indicate that a mesoscopic approach can be useful for studying the influence of the concrete internal structure on the macroscopic mechanical response. However, for larger scales it might not be viable to represent the entire domain in mesoscale. By dividing the domain in subdomains, different scales can be applied giving a better refinement to the most critical stresses areas.

Therefore, the present work proposes a concurrent two-scale (macro and mesoscale) approach for HSC, where the macroscopic and mesoscopic meshes are coupled via Coupling Finite Elements (CFEs) [12]. A linear elastic model with homogenized elastic properties is used for the macroscale whereas a three-phase material composed of coarse aggregate, mortar matrix and the interfacial transition zone (ITZ) with nonlinear behavior models are assumed for the mesoscopic level. The FEM analysis is

preceded by a mesh fragmentation technique (MFT) [13] that places high-aspect ratio elements between regular elements in the mesoscopic region. The coarse aggregates are randomly generated from a grading curve and placed in the mesoscale subdomain, using the “take-and-place” method [14]. Individual phase properties required for the mesoscale model are derived from homogenized properties using a mix theory for concrete [14]. The combination of such techniques should result in a model fit to evaluate the aggregate influence on HSC.

## 2 TWO-SCALE MODELING

### 2.1 Random aggregate generation

In this work, the random generation of coarse aggregates is accomplished by the employment of “take-and-place” method [14]. The aggregate particles are represented by regular octagons placed in the mortar matrix with size varying within a range. The volume of particles with a given diameter interval ( $d_{min} < d_a < d_{max}$ ) can be obtained from the passing percentage in a grading curve or assumed from the theoretic Fuller curve, which is based on the best compaction distribution [11,14].

In this iterative method, the octagon shapes are inscribed in circles with a random radius within the range. Thus, each circle must be placed inside the matrix respecting a distance from the already placed octagons as well as from the geometry boundaries. Figure 1 illustrates the distance constraints for the random aggregate placing with respect to parameter  $\lambda$ .

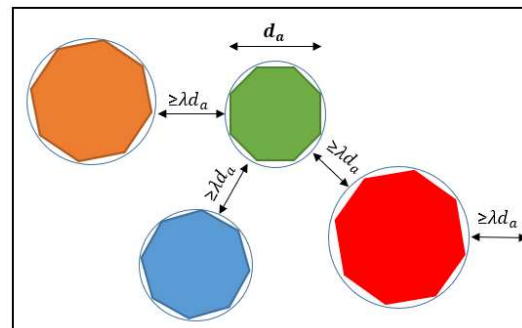


**Figure 1:** Random generation of coarse aggregates based on take-and-place method.

## 2.2 Mesh fragmentation technique

The mesh fragmentation technique (MFT) proposed by Manzoli et al. [13] is based on the use of interface solid finite elements to represent the crack propagation potential paths. The MFT allows representing the crack initiation, propagation and coalescence, considering the individual behavior of each phase as well as their mutual interactions at the mesoscale level of HSC. This discrete approach is based on the insertion of pairs of triangular FEs with high aspect ratio between adjacent regular elements of a conventional FE mesh.

The MFT has been successfully used to model the bond-slip behavior of reinforcing bars embedded in concrete, propagation of 3D cracks induced by shrinkage in drying soils and also 2D mesoscale modeling of concrete [11,13,15].

In the particular case of HSC, where the cement paste has a high strength and the cracks might propagate through the aggregates, the mesh fragmentation technique also must be applied to the aggregate elements and not only to the matrix and ITZ as it was observed in the simulation of regular strength concrete [15].

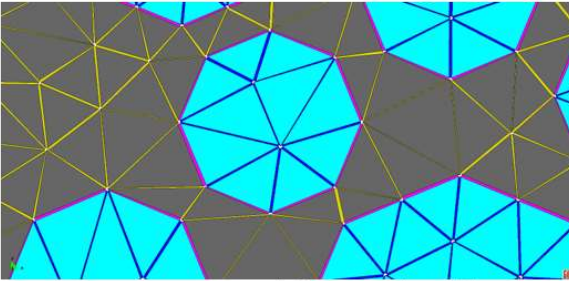


**Figure 2:** Concrete mesh fragmentation with aggregate interface element (blue), matrix interface element (yellow) and ITZ element (pink).

## 2.3 Coupling finite element

The concurrent multiscale model adopted to represent the HSC results in a high refinement to the mesoscale region and a low refinement to the macroscale domain (homogeneous region of the specimen). Therefore, this simulation usually involves non-matching meshes, for which CFEs are employed in this work to ensure a rigid coupling between these initially independent meshes, as shown in Figure 3.

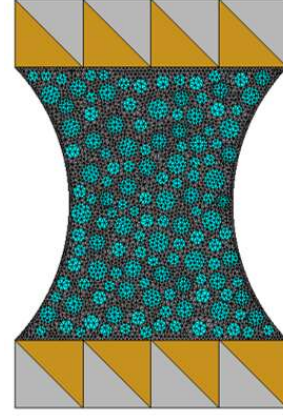


**Figure 3:** Dog-bone specimen with coupling elements (in yellow) linking the macro (light grey) and mesoscale (dark grey) meshes.

Proposed by Bitencourt et al. [12], the coupling technique is based on the use of CFEs, by ensuring the continuity of displacement and stress fields between independent (non-matching) meshes.

According to Bitencourt et al. [12] the global internal force vectors and stiffness matrix are obtained by Equations 1 and 2:

$$\mathbf{F}^{int} = A_{e=1}^{nel\Omega_1} (\mathbf{F}_e^{int})_{\Omega_1} + A_{e=1}^{nel\Omega_2} (\mathbf{F}_e^{int})_{\Omega_2} + A_{e=1}^{nelc} (\mathbf{F}_e^{int})_c \quad (1)$$

$$\mathbf{K} = A_{e=1}^{nel\Omega_1} (\mathbf{K}_e)_{\Omega_1} + A_{e=1}^{nel\Omega_2} (\mathbf{K}_e)_{\Omega_2} + A_{e=1}^{nelc} (\mathbf{K}_e)_c \quad (2)$$

where  $A$  is the finite element assembly operator, and  $\Omega_1$ ,  $\Omega_2$  and  $C$  are related to the subdomains from the macroscale region, mesoscale region, and the interaction between them. Details about the coupling FE technique can be found in Bitencourt et al. [12].

## 2.4 Constitutive damage model

A tension damage model is used to describe the concrete cracking process. In this way, a damage variable,  $d$ , is used to degrade all the components of the effective stress tensor,  $\bar{\boldsymbol{\sigma}}$ , and obtain the current stress tensor,  $\boldsymbol{\sigma}$ , according to the tension stress component normal to the base of the interface element,  $\bar{\sigma}_{nn}$ , as described by Equation 3.

$$\boldsymbol{\sigma} = \begin{cases} (1-d)\bar{\boldsymbol{\sigma}} & \text{if } \bar{\sigma}_{nn} > 0 \\ \bar{\boldsymbol{\sigma}} & \text{if } \bar{\sigma}_{nn} \leq 0 \end{cases} \quad (3)$$

The effective stress tensor is computed from

the current strain tensor,  $\boldsymbol{\varepsilon}$ , such as:

$$\bar{\boldsymbol{\sigma}} = \mathbf{C} : \boldsymbol{\varepsilon} \quad (4)$$

where  $\mathbf{C}$  is the fourth order elastic tensor.

This damage model has been formulated in the framework of the implicit-explicit integration scheme (IMPL-EX), as proposed by Oliver et al. [16].

## 2.5 Parameters

As a constitutive tensile damage model is employed to represent the crack propagation, two fracture parameters are necessary: tensile strength and fracture energy. Unfortunately, such values to be used at mesoscale are not often directly obtained from experimental results, but only for the concrete as a homogeneous material. Therefore, tensile strength and fracture energy for each phase of the concrete constituent materials and respective ITZs must be determined from the general known parameters and available data found in the literature.

In order to obtain these parameters, some assumptions were made based on researches regarding high strength concrete behavior. One significant consideration taken into account were that although the aggregate type has a high influence on the concrete compression strength, it impacts the flexural or tensile strength minimally [4,6]. Results regarding flexural strength of concrete indicate that the rock strength has very little influence compared to the cement matrix and the ITZ [4-6]. This is an encouraging data for the application of a tensile damage model because the response is not expected to be very sensitive to the rock strength, which is usually not tested for concrete production purposes.

Therefore, estimated parameters based on literature average values for common aggregate should be acceptable for the simulation.

For the elastic properties, once the homogeneous values are known and the aggregate can be assumed, the matrix elastic property (elastic modulus and Poisson's ratio) can be estimated based on the rule of mixture, as proposed by Counto [22], which considers the concrete as a two-phase material (aggregate and

matrix), using the following expression:

$$\frac{1}{E_{hom}} = \frac{1 - \sqrt{V_{agg}}}{E_{mat}} + \frac{1}{\left(\frac{1 - \sqrt{V_{agg}}}{\sqrt{V_{agg}}}\right) E_{mat} + E_{agg}} \quad (5)$$

where  $E_{hom}$  is the homogenized (effective) Young's modulus or Poisson's ratio.  $E_{mat}$  and  $E_{agg}$  are the Young's modulus or Poisson's ratio of the matrix and aggregate, respectively.  $V_{agg}$  is the volume fraction of aggregate, expressed as a percentage.

Also, for HSC, the ITZ was found to present 30% to 50% less tensile strength than the matrix [4-5]. Therefore, the homogeneous tensile strength of concrete was defined as the average value of the matrix, ITZ and aggregate tensile strength, as the following expressions:

$$f_{itz} \cong 0.7 \times f_{mat} \quad (6)$$

$$f_{hom} = \frac{f_{itz} + f_{mat} + f_{agg}}{3} \quad (7)$$

where  $f_{itz}$ ,  $f_{mat}$  and  $f_{agg}$  are the ITZ, matrix and the aggregate tensile strength.  $f_{hom}$  is the homogenized (effective) tensile strength.

The same expression can be used to obtain the respective fracture energies of each phase.

## 3 RESULTS

### 3.1 Dog-bone specimen

In this example, a dog-bone specimen was tested in an attempt to perform a parametric analysis of the HSC in mesoscale, varying the aggregate tensile strength and the corresponding ITZ percentage to evaluate how it affects the response. First, using the previously described expressions, all the parameters were set for a concrete with the following homogenized properties: 65 MPa compressive strength, 4 MPa tensile strength, 46 GPa elastic modulus and 0.122 N/mm fracture energy. The specimen has 150mm of height, 100mm of width and 100mm of depth. In the middle of the specimen (neck zone), the cross-section width is reduced to 60mm.

The coarse aggregates are randomly generated

and placed one-by-one into the matrix, assuming the Fuller's grading curve distribution, with a constant volume fraction of 35% and aggregate diameter size varies from 4mm to 8mm. The elastic and inelastic properties assigned to the aggregate were those related to the limestone, which is an average strength rock very used as an aggregate [17-19]. By assuming the aggregate properties and considering the ITZ strength and energy fracture as 70% of the matrix respective parameters, all the individual phases were set.

Then, for the study purposed, only the aggregate tensile strength ( $f_{agg}$ ) varied from 3 MPa to 6MPa and every other parameter remained unchanged, as shown in Table 1.

**Table 1:** Interface elements fracture properties.

Phase	$f_t$ (MPa)	$G_f$ (N/mm)
Aggregate - Aggregate	3.0 to 6.0	0.100
Matrix - Matrix	5.9	0.158
ITZ	4.1	0.111

The results obtained are shown in Figures 4 to 6. When the aggregate is much weaker than the matrix ( $f_{agg} = 3$  and  $f_{agg} = 4$ ), the predominant crack tends to be very straight and crosses the aggregates, as shown in Figure 4(a-b). However, increasing the aggregate strength, the fracture becomes more diffuse, deviating from the aggregates, as illustrated in Figure 4(c-d).

Additionally, when the aggregate is the strongest phase, it no longer impacts the response, as it can be observed by the similarity of curves in Figure 6. However, it is possible to note in the load-displacement curves illustrated in Figures 5 and 6 that the intermediate tensile strength values assumed for aggregates ( $f_{agg} = 4$  and  $f_{agg} = 5$ ) can affect the peak-load of the structural responses. Thus, it is reasonable to state that in the case of HSC, where, in general, the matrix tensile strength is higher than the aggregate tensile strength, the aggregates are the weakest phase of the composite, since decreasing the aggregate tensile strength leads to a significant peak resistance reduction.

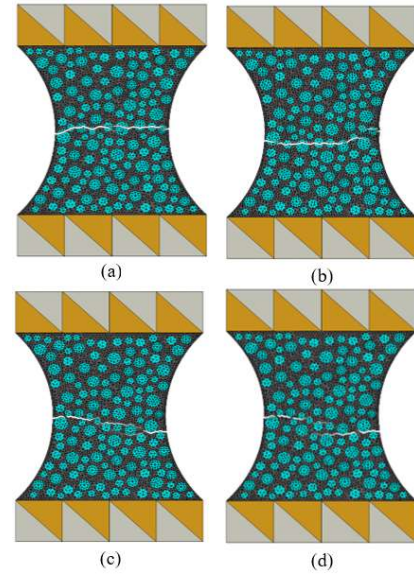


**Figure 4:** Fracture in the dog-bone specimen with aggregate tensile strength equal to (a) 3 MPa; (b) 4 MPa; (c) 5 MPa; and (d) 6 MPa.

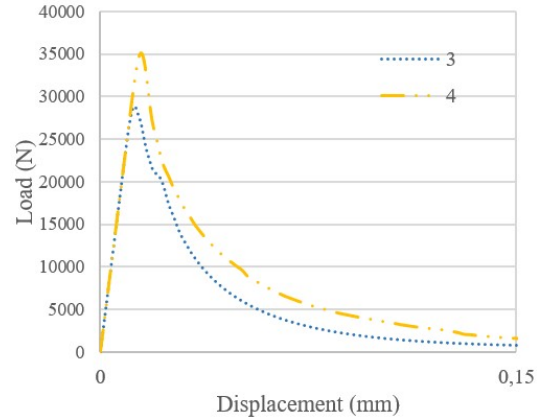


**Figure 5:** Load x displacement curves for dog-bone specimen with different aggregate tensile strengths.

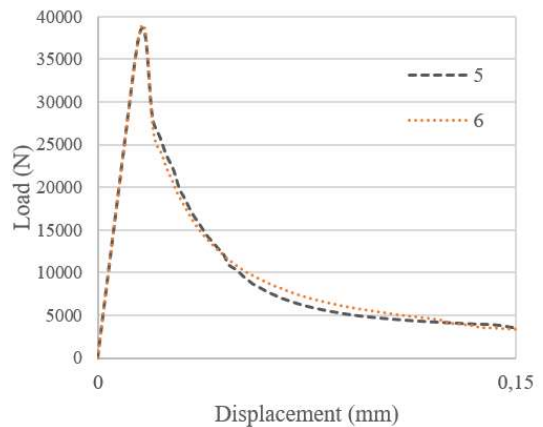


**Figure 6:** Load x displacement curved for dog-bone specimen with different aggregate tensile strengths.

The next parameters analyzed were the ITZ tensile strength ( $f_{ITZ}$ ) and fracture energy

( $G_{f_{ITZ}}$ ), respectively, which are described as a percentage of the matrix tensile strength ( $f_{mat}$ ) and fracture energy ( $G_{f_{mat}}$ ), keeping the other properties constant,  $f_{ITZ}$  and  $G_{f_{ITZ}}$  are varied from 50% to 80% of the matrix properties as shown in Table 2.

Figure 7 illustrates the deformed configuration of the dog-bone simulated. It is possible to note that the ITZ can also influence the fracture pattern. In the cases where the ITZ is relatively stronger, it facilitates the fracture process through aggregates. When it is much weaker than the matrix, the fracture tends to become more inclined. That condition can indirectly affect the fracture energy, which is by definition the energy required to fracture one unity of area. That might explain why the curve with 50% of the matrix strength in Figure 8 seems more ductile than the curve for 80% strength shown in Figure 9.

**Table 2:** Interface elements fracture properties.

Phase	$f_t$ (MPa)	$G_f$ (N/mm)
Aggregate - Aggregate	4.0	0.100
Matrix - Matrix	5.9	0.144
	2.95	0.079
ITZ	3.54	0.095
	4.20	0.111
	4.72	0.1264

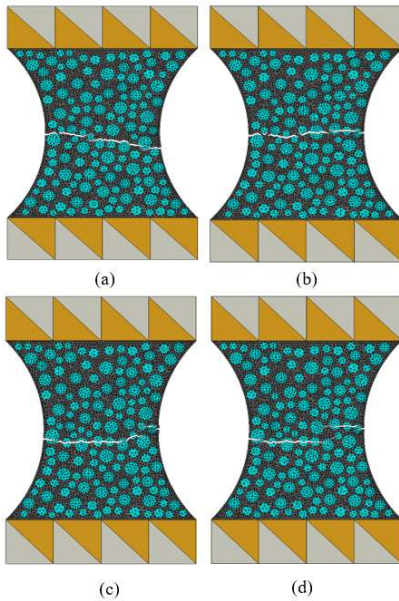


**Figure 7:** Fracture in the dog-bone specimen with ITZ tensile strength calculated as (a) 50%; (b) 60%; (c) 70%; and (d) 80% of the matrix strength.

On the other hand, when the ITZ tensile strength assumes between 60% and 70% of the matrix tensile strength, the response seems to be more stable. In fact, the ITZ influence appears to be more complex, justifying all the researches ongoing on this subject.

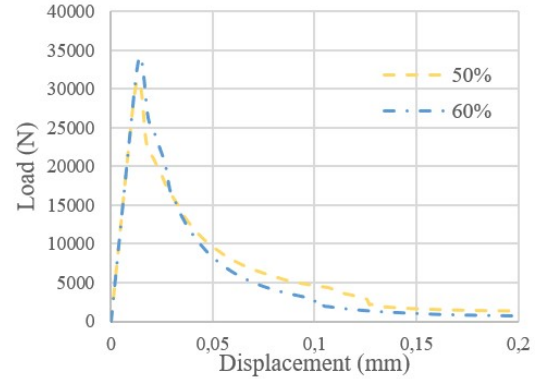


**Figure 8:** Load x displacement curve with ITZ tensile strength calculated as 50% and 60% of the matrix strength.

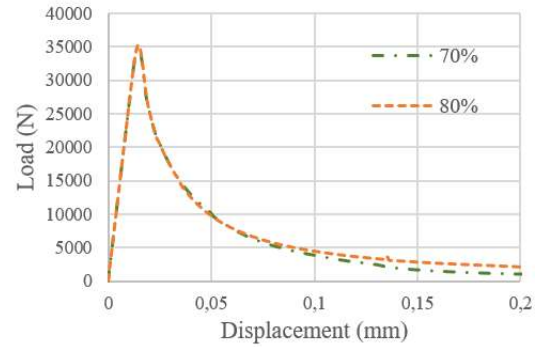


**Figure 9:** Load x displacement curve with ITZ tensile strength calculated as 70% and 80% of the matrix strength.

### 3.2 Three-point bending beams

In this second example, the HSC beams experimentally tested by Siregar et al. [20] are numerical simulated, employing the concurrent multiscale model proposed.

#### 3.2.1 Description of the beams experimentally tested by Siregar et al. [20]

The experimental evaluation of the aggregate grading influence in HSC was performed by Siregar et al. [20] in notched beams with 850mm length, 800mm mid span, 100x100mm of cross-sectional area and 3mm notch, as shown in Figure 10. The crack mouth opening displacement (CMOD) and deflection were measured by the authors [20].

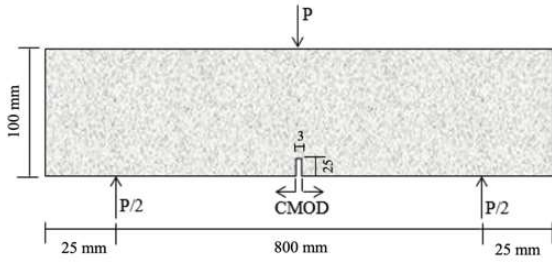


**Figure 10:** Notched concrete beam experimentally tested by Siregar et al. [20].

Three different coarse aggregate grading and two water to binder ratio were used in the production of the concrete. The coarse aggregates used was within the range of 5mm to 16mm. The grading A has the minimum average aggregate diameter ( $A_D$ ), while grading B has the maximum  $A_D$ , as can be observed in Figure 11.

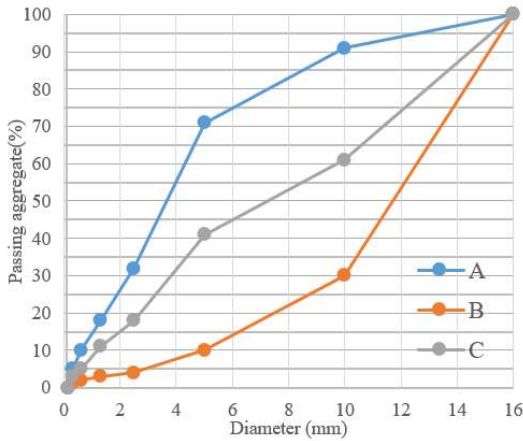


**Figure 11:** Coarse aggregate grading curves (adapted from Siregar et al. [20]).

The two different water/binder ratios are referred to as Mixes 1 and 2. The first total w/b ratio is 0.2 and the second is 0.3. Therefore, both mixes result in high strength concretes, but Mix 1 has a higher compressive strength ( $f_{ck}$ ) than Mix 2. Table 3 displays the properties of hardened concrete for all w/b and grading tested.

**Table 3:** Compressive strength and fracture energy of each type of concrete used for the experimental testing (adapted from Siregar et al [20]).

Mix	$f_{ck}$ (MPa)	$G_f$ (N/mm)
A1	85.2	0.0938
B1	97.6	0.1499
C1	94.8	0.1267
A2	68.2	0.0851
B2	66.0	0.1465
C2	68.4	0.1343

### 3.2.2 Numerical analyses

In this work, the beams experimentally tested by Siregar et al. [20] to study the influence of aggregate grading in HSC are numerically simulated employing the main ingredients of the concurrent multiscale approach proposed. Figure 12 illustrates the multiscale representation of the beam, in which only a region near the notch is represented in mesoscale.

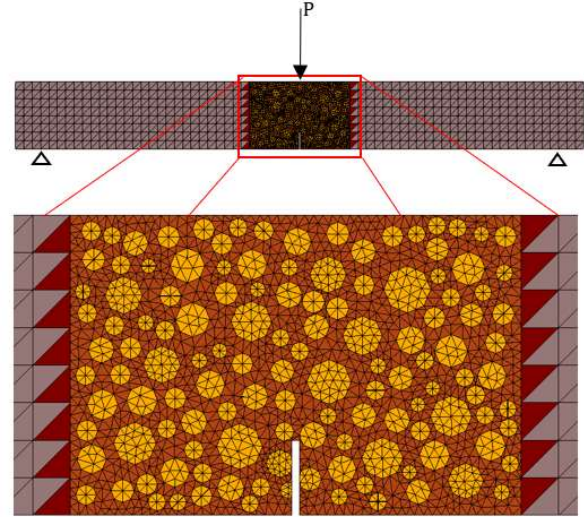


**Figure 12:** Notched concrete beam in mesoscale with CFE (in red) providing coupling between non-conform meshes.

To verify the capacity of the model to capture the effect of using different grading curves, the parameters set to the aggregate, matrix and transition zone interface were the same for specimens made from the same mix (w/c ratio). Even though each specimen presented its own compressive strength and fracture energy (as shown in Table 3), the mean values for each mix were calculated. That means, specimens A1, B1 and C1 were assigned the same  $f_t$  and  $G_f$  parameters, so that the only difference would be the aggregate distribution inside the specimen. The same occurred with the specimens A2, B2 and C2.

As previously mentioned, the constitutive damage model is based on the material tensile strength ( $f_t$ ), so using the correlation provided by Brazilian Standard ABNT/NBR 6118 [21], the mean  $f_t$  for mix 1 and 2 were calculated. Using the same considerations from the dog-bone specimen, the particular values for each interfacial material was calculated, as shown in

Table 4.

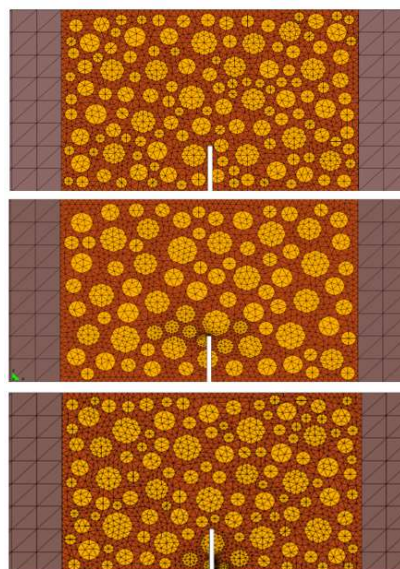
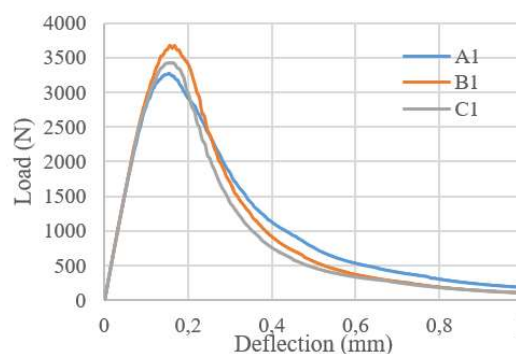
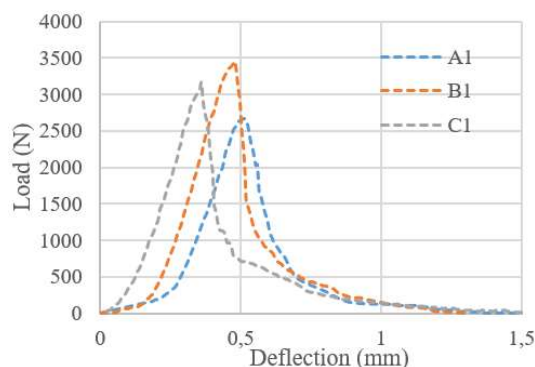
**Table 4:** Interface elements fracture properties.

Mix 1		
Phase	$f_t$ (MPa)	$G_f$ (N/mm)
Aggregate - Aggregate	4.0	0.100
Matrix - Matrix	5.9	0.158
ITZ	4.2	0.111
Mix 2		
Aggregate - Aggregate	4.0	0.100
Matrix - Matrix	4.7	0.140
ITZ	3.3	0.100

Once the parameters have been set, the analysis proceeded to the mesoscale model generation illustrated in Figure 13, where there is a visible difference in the grading. As a 2D approach is adopted, 3 different models were generated for each grading in order to minimize the Influence of the distribution. The curves presented in the next figures are the mean responses obtained.

The simulation for Mix 1 demonstrated that indeed, the granulometry has an impact in the high strength concrete mechanical behavior. The results in Figures 14 to 17 suggest that the best performance in terms of peak load was achieved by grading B, which has the maximum average particle diameter. The experimental results for deflection also present grading B as the best response, followed by grading C and A. The maximum peak load for the numerical and experimental analysis is very close, however, the experimental test seems to catch a bigger gap between the different grading.

The numerical and experimental CMOD response curves illustrated in Figures 16 and 17 are also in agreement, as grading C has a higher peak load than grading A in both cases. These results suggest that high strength concretes with greater average diameters are able to dissipate more energy than HSC with smaller average diameter.

**Figure 13:** Mesoscale models for gradings A, B and C, respectively.**Figure 14:** Numerical load x deflection curves for specimens A1, B1 and C1.**Figure 15:** Experimental load x deflection curved for specimens A1, B1 and C1 (adpated from [20]).

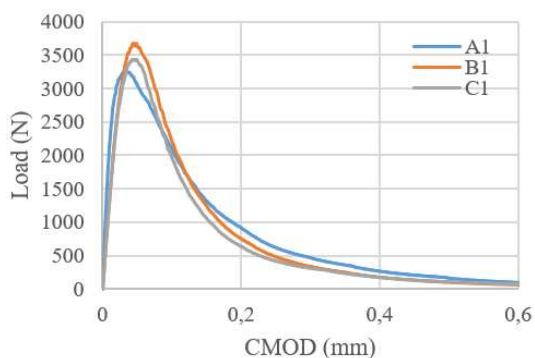


**Figure 16:** Numerical load x CMOD curves for specimens A1, B1 and C1.

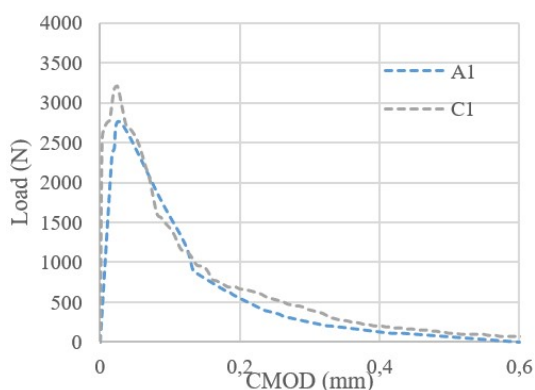


**Figure 17:** Experimental load x CMOD curves for specimens A1, B1 and C1 (adapted from [20]).

From the post-process results in Figure 18, it is possible to notice that in all cases the fractures propagated through the aggregate, which was also reported to happen in the experimental analysis.

The cracking formation exhibited a very inclined path, as observed in the actual specimen by Siregar et. al (2017), which is pictured in Figure 19. The numeric model was able to represent it by assigning the aggregate and ITZ inferior tensile strength and energy fracture.

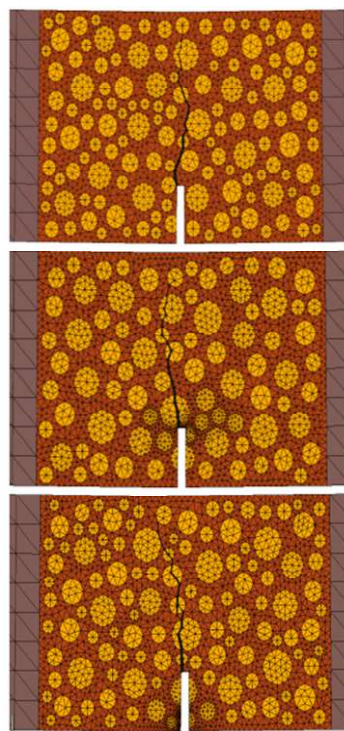


**Figure 18:** Fracture process in specimens A1, B1 and C1, respectively.

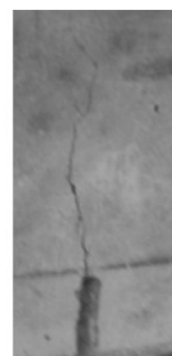


**Figure 19:** Crack path of specimen with 0.2 w/b ratio (Siregar et al. [20]).

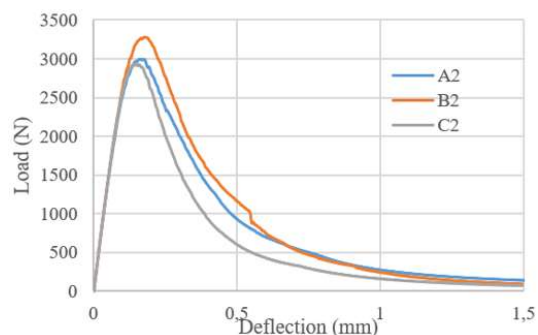


**Figure 20:** Numerical load x deflection curves for specimens A2, B2 and C2.

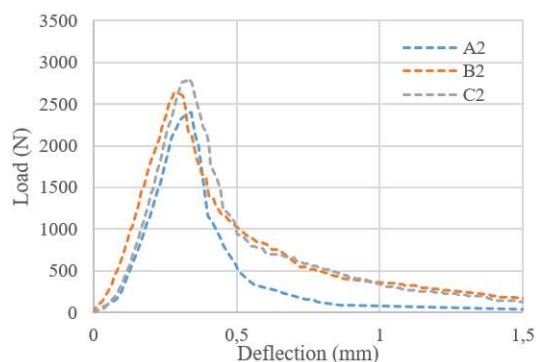


**Figure 21:** Experimental load x CMOD curves for specimens A2, B2 and C2 (adapted from [20]).

The simulation for Mix 2 (Figures 20 to 23) resulted in a response similar to Mix 1, where grading B presented a slightly higher peak load and the residual force was close for all granulometries. A possible reason why the grading with bigger average aggregate diameter presented a higher peak load in both cases is because of the larger space between aggregates (the weakest phase), resulting in a fracture path with greater length. Besides the aggregate distribution, it was noticed that the change in the w/b ratio also affected the response, once for Mix 2 grading A presented better response than grading C, as opposed to what was observed in Mix 1.

The w/b ratio sensitivity was also observed by Siregar et al. (2017) suggesting that a reduction in the coarser grain size in the mix is associated with lower fracture energy.

However, compared to the previous analysis, the fracture inclination (Figure 24) was much smaller, which can be explained by the fact that the w/b ratio in Mix 2 was higher, therefore, aggregate, and matrix had closer strength, as shown in Table 4.

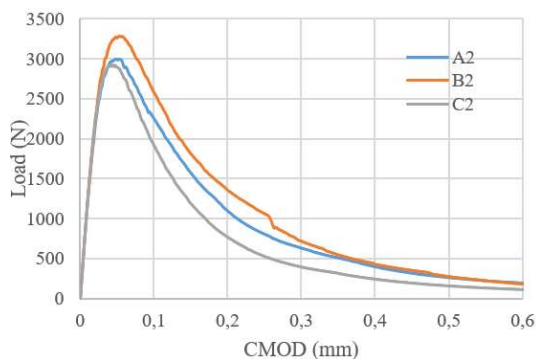


**Figure 22:** Numerical load x CMOD curves for specimens A2, B2 and C2.

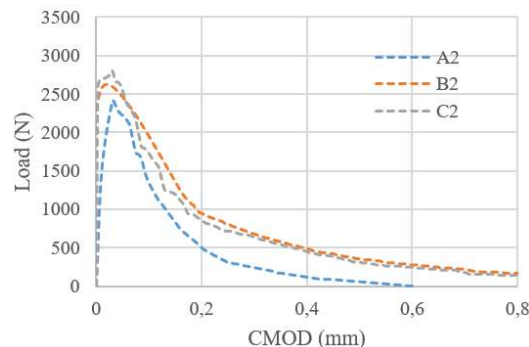


**Figure 23:** Experimental load x CMOD curves for specimens A2, B2 and C2 (adapted from [20]).

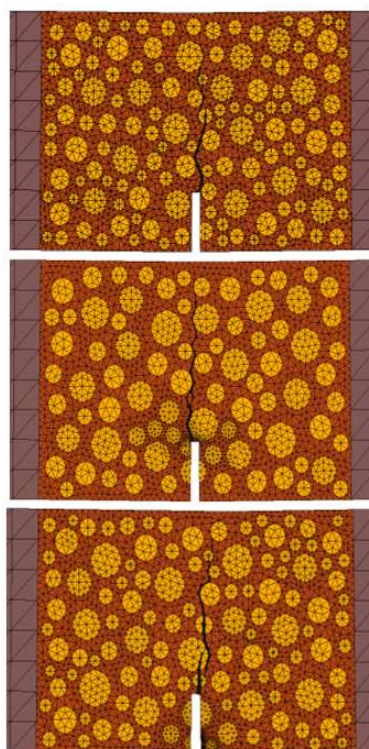


**Figure 24:** Fracture process in specimens A2, B2 and C2, respectively.

## 4 CONCLUSIONS

This paper analyzed the mechanical behavior of high strength concrete using a two-scale model based on the application of a mesh fragmentation technique. First, a sensitivity analysis of a dog-bone specimen was performed and then the model was applied to simulate the experiment conducted by Siregar et al. [20] in notched beams. The main conclusions drawn from these analyses were:

- The coupling finite element can be used to construct concurrent multiscale model for modeling HSC, by adopting homogeneous

material properties at macroscale domain, and three-phase material at mesoscopic domain.

- Different responses were obtained for HSC made with different tensile strength aggregates. It was observed that decreasing the aggregate tensile strength leads to a significant peak resistance reduction.
- The ITZ influence was of little significance in terms of peak resistance but it was noticeable in the post-process fracture path. The stronger the ITZ, the more straight the fracture.
- As observed in experimental studies, for each w/b ratio, specimens were assigned the same elastic and inelastic parameters and still, the response was different, indicating sensitivity to aggregate distribution.
- It was observed that the mix with higher strength (Mix 1) was slightly more sensitive to the grading than the other w/b ratio mix. It can be explained by the fact that the phases had greater disparity.
- The fracture propagates through aggregates in almost all simulations, even in Mix 2, where the ITZs happened to be more weakened than the aggregates. That was only possible due to the fragmentation technique applied to all phases of the material at mesoscale.
- By analyzing the post-process configuration, it is visible that in Mix 1, which has the stronger mortar, the fracture path tends to deviate more from the center of the notch due to the "search" for the weakest phase (aggregate). In mix 2 that behavior is much subtler.

## 5 REFERENCES

- [1] Kılıç, A.; Atiş, C.D.; Yaşar, E.; Özcan, F. 2003. High-strength lightweight concrete made with scoria aggregate containing mineral admixtures. *Cement and Concrete Research*. Vol. 33, Issue 10, pp. 1595-1599.
- [2] Yazıcı, H. 2007. The effect of curing conditions on compressive strength of ultra high strength concrete with high volume mineral admixtures. *Building and Environment*. Vol. 42; pp. 2083-2089.
- [3] Poon, C.S.; Lam, L.; Wong, Y.L. 2000. A study on high strength concrete prepared with large volumes of low calcium fly ash. *Cement and Concrete Research*. Vol 30, pp. 447-455.
- [4] Giaccio, G.; Rocco, C.; Violini, D.; Zappitelli, J.; Zerbino, R. 1992. High Strength Concretes Incorporating Different Coarse Aggregates. *ACI Materials Journal*. 89(3):242-246.
- [5] Chen, B.; Liu, J. 2004. Effect of the aggregate on the Fracture behavior of high strength concrete. *Construction and Building Materials*. Vol. 18; pp. 585-590.
- [6] Wu, K.; Chen, B.; Yao, W.; Zhang, D. 2001. Effect of coarse aggregate type on mechanical properties of high-performance concrete. *Cement and Concrete Research*. Vol. 31; pp.1421-1425.
- [7] Wang, X.F.; Yang, Z.J.; Yates, J.R.; Jivkov A.P.; Zhang, Ch. 2015. Monte Carlo simulations of mesoscale fracture modelling of concrete with random aggregates and pores. *Construction and Building Materials*. Vol. 75, pp. 35-45.
- [8] Zhou, R.; Song, Z.; Lu, Y. 2017. 3D mesoscale finite element modelling of concrete. *Computers & Structures*. Vol. 192, pp. 96-113.
- [9] Huang, Y.J.; Yang, Z.J.; Chen, X.W.; Liu, G.H. 2016. Monte Carlo simulations of meso-scale dynamic compressive behavior of concrete based on X-ray computed tomography images. *International Journal of Impact Engineering*. Vol. 97, pp. 102-115.
- [10] Song, Z.; Lu, Y. 2012. Mesoscopic analysis of concrete under excessively high strain rate compression and implications on interpretation of test data. *International Journal of Impact Engineering*. Vol. 46,

pp. 41-55.

- [11] Rodrigues, E.A.; Manzoli, O. L.; Bitencourt Jr., L.A.G.; Bittencourt, T.N. 2016. 2D mesoscale model for concrete based on the use of interface element with a high aspect ratio. *International Journal of Solids and Structures*, Vol. 94-95; pp. 112-124.
- [12] Bitencourt Jr., L.A.G.; Manzoli O.L.; Prazeres, P.G.C.; Rodrigues, E.A.; Bittencourt, T.N. 2015. A coupling technique for non-matching finite element meshes. *Comput. Methods Appl. Mech. Engrg.* 290, 19-44.
- [13] Manzoli, O.L; Maedo, M.A.; Bitencourt Jr., L.A.G.; Rodrigues, E.A. 2016. On the use of finite elements with a high aspect ratio for modeling cracks in quasi-brittle materials. *Engineering Fracture Mechanics*. 153, pp. 151-170
- [14] Wriggers, P.; Moftah, S.O. 2006. Mesoscale models for concrete: homogenization and damage behaviour. *Finite Elements in Analysis and Design*. 42, 623-636.
- [15] Rodrigues, E.A.; Manzoli, O.L.; Bitencourt Jr., L.A.G.; Bittencourt, T.N.; Sánchez, M. 2018. An adaptive concurrent multiscale model for concrete based on coupling finite elements. *Computer Methods in Applied Mechanics and Engineering*. Vol. 328, pp. 26-46.
- [16] Oliver, J.; Huespe, A.E.; Cante, J.C. 2008 An implicit/explicit integration scheme to increase computability of non-linear material and contact/friction problems. *Comput. Methods Appl. Mech. Engrg.* Vol. 197, pp.1865-1889.
- [17] Baykasoğlu, A.; Güllü, H.; Çanakçı, H.; Özbakır, L. 2008. Prediction of compressive and tensile strength of limestone via genetic programming. *Expert Systems with Applications*. Vol. 35, pp. 111-123.
- [18] You, M. 2015. Strength criterion for rocks under compressive-tensile stresses and its application. *Journal of Rock Mechanics and Geotechnical Engineering*. Vol.7, pp. 434-439.
- [19] Perras, M.A.; Diederichs, M.S. 2014. A Review of the Tensile Strength of Rock: Concepts and Testing. *Geotechnical and Geological Engineering*. Vol.32, pp. 525-546.
- [20] Siregar, A.P.N.; Rafiq, M.I. and Mulheron, M. 2017. Experimental investigation of the effects of aggregate size distribution on the fracture behaviour of high strength concrete. *Construction and Building Materials*. Vol. 150; pp. 252-259.
- [21] ABNT NBR 6118. 2014. Design of concrete structures: procedure, Rio de Janeiro, Brazil.
- [22] Counto, U.J. 1964. The effect of the elastic modulus of the aggregate on the elastic modulus, creep and creep recovery of concrete. *Mag. Concr. Res.* 16 (48), 129–138.